



Uncovering bound states in the continuum in InSb nanowire networks

D. Martínez^{a,*}, P.A. Orellana^b, L. Rosales^b, J. Dolado^c, M. Amado^d, E. Diez^e,
F. Domínguez-Adame^a, R.P.A. Lima^{a,f,g}

^a GISC, Departamento de Física de Materiales, Universidad Complutense, E-28040 Madrid, Spain

^b Departamento de Física, Universidad Técnica Federico Santa María, Casilla 110 V, Valparaíso, Chile

^c ESRF, The European Synchrotron, 71 Avenue des Martyrs, Grenoble 38043, France

^d Nanotechnology Group, USAL-Nanolab and IUFFyM, Universidad de Salamanca, E-37008 Salamanca, Spain

^e Nanotechnology Group, USAL-Nanolab, Universidad de Salamanca, E-37008 Salamanca, Spain

^f GFTC, Instituto de Física, Universidade Federal de Alagoas, Maceió AL 57072-970, Brazil

^g IES, Departamento de Electrónica Física, Ingeniería Eléctrica y Física Aplicada, ETSIT, Universidad Politécnica de Madrid, Avenida Complutense 30, E-28040 Madrid, Spain

ARTICLE INFO

Editor: M.W. Wu

Keywords:

Bound states in the continuum
InSb nanowire networks
Spin polarization

ABSTRACT

Bound states in the continuum (BICs) are exotic, localized states even though their energy lies in the continuum spectra. Since its discovery in 1929, the quest to unveil these exotic states in charge transport experiments remains an active pursuit in condensed matter physics. Here, we study charge transport in InSb nanowire networks in the ballistic regime and subject to a perpendicular magnetic field as ideal candidates to observe and control the appearance of BICs. We find that BICs reveal themselves as distinctive resonances or antiresonances in the conductance by varying the applied magnetic field and the Fermi energy. We systematically consider different lead connections in hashtag-like nanowire networks, finding the optimal configuration that enhances the features associated with the emergence of BICs. Finally, the investigation focuses on the effect of the Rashba spin-orbit interaction of InSb on the occurrence of BICs in nanowire networks. While the interaction generally plays a detrimental role in the signatures of the BICs in the conductance of the nanowire networks, it opens the possibility to operate these nanostructures as spin filters for spintronics. We believe that this work could pave the way for the unambiguous observation of BICs in charge transport experiments and for the development of advanced spintronic devices.

1. Introduction

Bound states in the continuum (BICs) are spatially localized states or waves whose energy or frequency lies within a continuum spectrum of propagating modes. Von Neumann and Wigner proposed the existence of these exotic and counterintuitive states in the earlier days of quantum mechanics [1]. They constructed a spatially oscillating attractive potential and solved the corresponding Schrödinger equation, finding a truly localized state above the potential barrier as a result of destructive interference. Much later, Stillinger and Herrick reexamined and extended these ideas in the context of atoms and molecules [2].

The occurrence of BICs is related to the dynamics of coherent waves, and therefore, they have been thoroughly studied not only in atoms and molecules [2–4] but also in areas of optics and photonics [5–10], plasmonics [11–14], acoustics [15–18] and nanoelectronics [19–24], to name a few (see Refs. [25–28] for comprehensive reviews on BICs). Since the pioneering work by Plotnik et al. on the symmetry-protected

BICs in an array of parallel dielectric single-mode waveguides fabricated of fused silica [5], much progress have been achieved in the observation and characterization of BICs in photonic structures [29–31].

However, signatures of BICs in charge transport experiments remain elusive and less explored in the literature. Recent advances in nanotechnology have made it possible to conceive and fabricate quantum devices that support BICs. In this context, Albo et al. made use of intersubband photocurrent spectroscopy to demonstrate that a BIC exists above (Ga,In)(As,N) / (Al,Ga) as quantum wells that arises from the hybridization of nitrogen-related defect states and the extended states of the conduction band [32]. Nöckel investigated theoretically the ballistic electron transport across a quantum dot in a weak magnetic field [33]. Resonances in the transmission were found to get narrower upon decreasing the magnetic field, signaling the occurrence of BICs as the magnetic field vanishes. Therefore, the external magnetic field can control the coupling of the spatially localized state with extended

* Corresponding author.

E-mail address: dunmar01@ucm.es (D. Martínez).

<https://doi.org/10.1016/j.physe.2024.116145>

Received 20 May 2024; Received in revised form 29 October 2024; Accepted 29 October 2024

Available online 7 November 2024

1386-9477/© 2024 The Authors. Published by Elsevier B.V. This is an open access article under the CC BY-NC-ND license (<http://creativecommons.org/licenses/by-nc-nd/4.0/>).

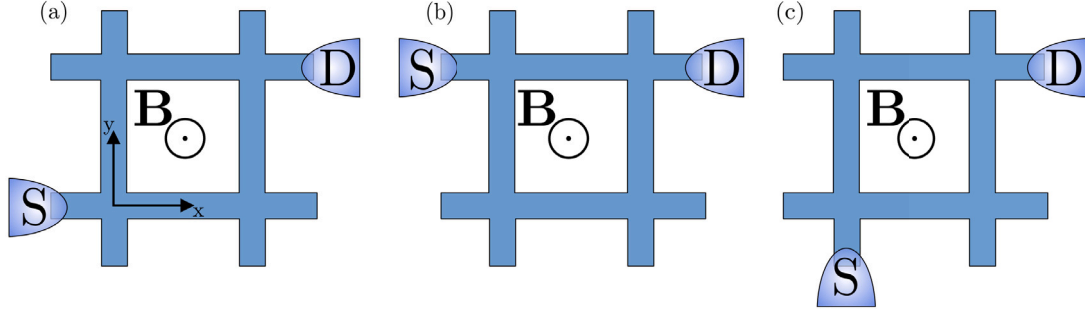


Fig. 1. Sketch of the configurationally different ways to attach the leads onto the nanowire network. S and D represents the source and drain leads. All the structures are threaded by a perpendicular magnetic field.

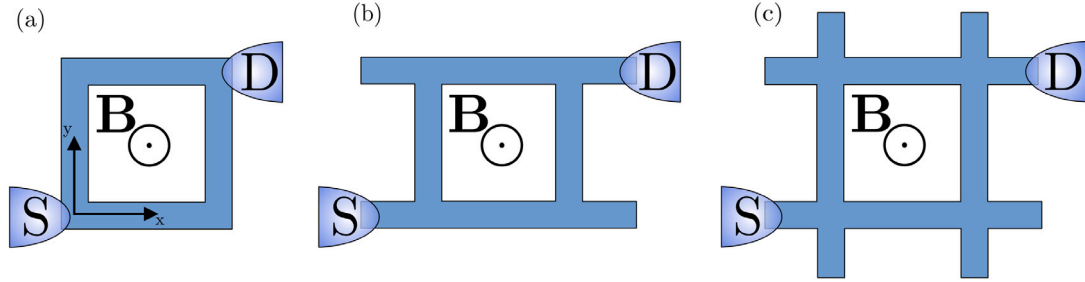


Fig. 2. Sketch of the configurationally different geometries of the nanowire network. S and D represents the source and drain leads. All the structures are threaded by a perpendicular magnetic field.

states of the continuum energy spectrum in nanostructures. In double or triple quantum dots, the coupling between the BICs and the continuum energy states can be controlled by detuning the energy levels of each quantum dot using gate voltages [19,21], without the need of external magnetic fields. In this case, the appearance of BICs is identified by the occurrence of Fano resonances [34] in the transmission.

In this work, we investigate the impact of BICs on the conductance of InSb nanowire networks in the ballistic regime, aiming to provide new routes for their observation in charge transport experiments. These nanostructures present phase-coherence lengths exceeding several micrometers with Aharonov–Bohm oscillations up to five harmonics due to high crystalline quality [35]. In addition, InSb nanowires have been theorized to host Majorana zero modes [36] and are regarded as suitable candidates for topological quantum computing [37]. Inspired by a study in which two interacting quantum dots exhibited BICs [38], our investigation focuses on nanowire networks forming a hashtag pattern. In this configuration, the corners emulate the quantum dots, while the branches correspond to tunneling processes between them. Here, the dead-end chains connected to the corners allow us to control the interference among various electron paths that help us to set the energy of the BICs. The main goal of this research is to determine the optimal configuration, including the placement of the leads and whether and where to place the dead-end chains, to enable the unambiguous observation of the BICs. Finally, the effect of the strong Rashba spin–orbit interaction (SOI) of InSb nanowires on the BICs and the associated spin currents is studied.

2. Model Hamiltonian and method

We consider six different arrangements of leads and dead-end branches of the two-dimensional InSb nanowire network. All of them will have a hashtag structure, but different places where the leads are attached or the number of dead-end chains and where they are placed (see Figs. 1 and 2). Since the cross-section of the nanowires is small, the subbands are well separated in energy, and hence, the nanowires can be regarded as one-dimensional. By discretizing the

Ben Daniel–Duke Hamiltonian, the resulting equation of motion for the envelope function becomes equivalent to a tight-binding model with nearest-neighbor coupling. The hopping energy is $t = \hbar^2/(2m^*a^2)$, where m^* is the electron effective mass and a is the grid spacing. In this framework, the single-electron Hamiltonian can be cast in the form $\mathcal{H} = \mathcal{H}_{\text{leads}} + \mathcal{H}_{\text{sys}} + \mathcal{H}_c$ where

$$\mathcal{H}_{\text{leads}} = t_l \sigma_0 \sum_{l,j} (d_{l+1,j}^\dagger d_{l,j} + d_{l,j+1}^\dagger d_{l,j}) + \text{h.c.}, \quad (1a)$$

$$\begin{aligned} \mathcal{H}_{\text{sys}} = & \sum_{n,m} (\epsilon_{nm} \sigma_0 + g \mu_B B \sigma_z) c_{n,m}^\dagger c_{n,m} \\ & - \sum_{n,m} \left(t e^{-i m a B} \sigma_0 - \frac{i \alpha}{2} \sigma_y \right) c_{n+1,m}^\dagger c_{n,m} \\ & - \sum_{n,m} \left(t \sigma_0 + \frac{i \alpha}{2} \sigma_x \right) c_{n,m+1}^\dagger c_{n,m} + \text{h.c.} \end{aligned} \quad (1b)$$

Here, $d_{l,j} = (d_{l,j,\uparrow}, d_{l,j,\downarrow})^T$ is the annihilation operator of the leads at site $\{l, j\}$ of the lead while $c_{n,m} = (c_{n,m,\uparrow}, c_{n,m,\downarrow})^T$ is the annihilation operator of the nanowire networks at site $\{n, m\}$ of the hashtag pattern, t and t_l are the hopping energy in the network and the leads respectively, ϵ_{ij} is the site energy of the network taking the site energy of the leads as zero, α is the Rashba spin–orbit coupling, σ_0 is the 2×2 identity matrix and $\sigma_{x,y,z}$ are the Pauli matrices. The network is threaded by a magnetic field tuned to add a complex phase in hopping parameter along the x direction. Finally, \mathcal{H}_c describes the tunnel coupling between neighbor sites of the lead and the hashtag network, with hopping energy t_l and a complex phase when the sites are aligned along the x direction.

Since we are assuming that the phase coherence length is larger than the system size, the conductance of the device is calculated within the Landauer–Büttiker formalism in the ballistic regime as follows

$$G(E) = \frac{e^2}{h} \tau(E), \quad (2)$$

where $\tau(E)$ is the transmission coefficient at the Fermi energy E and $-e$ is the electron charge. Notice that we are neglecting the broadening of the Fermi–Dirac distribution function by taking $T = 0$ K. The transmission coefficient can be calculated straightforwardly with the aid of the transfer-matrix approach or the Green’s functions method

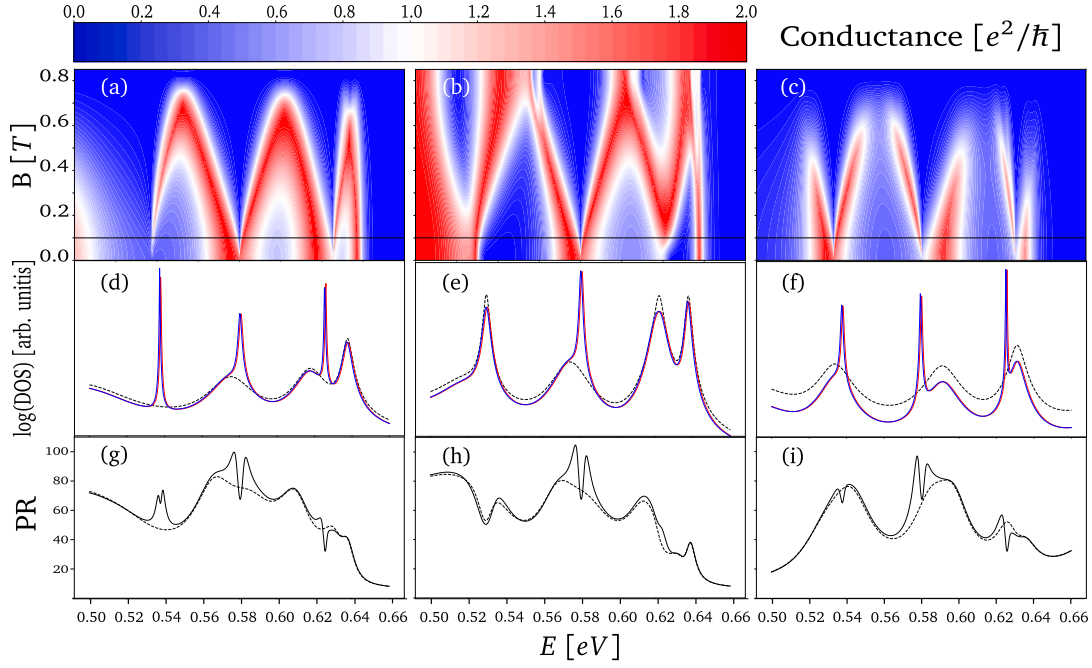


Fig. 3. Conductance of the nanowire network against the magnetic field B and the Fermi energy E . Panels (a), (b) and (c) correspond to the structures presented in Fig. 1(a), (b) and (c), respectively. The horizontal black line indicated the magnetic field at which the density of states and participation ratio are calculated ($B = 0.1$ T). Panels (d), (e) and (f) display the density of states with (solid line) and without (dashed line) magnetic field. Red (blue) line corresponds to the density of states with spin up (down). Panels (g), (h) and (i) represent the participation ratio with (solid line) and without (dashed line) magnetic field for the up spin projection.

(see Supplementary Material). Additionally, when there is a spin-flip mechanism as Rashba SOI, the conductance can be obtained as

$$G_{s,s'}(E) = \frac{e^2}{h} \tau_{s,s'}(E), \quad (3)$$

where $s, s' = \uparrow, \downarrow$ stand for the spin projections of the incoming and outgoing electron states, respectively. Therefore, we can define the spin polarization of the conductances as follows

$$P_S(E) = G_{\uparrow,\uparrow} + G_{\downarrow,\uparrow} - G_{\uparrow,\downarrow} - G_{\downarrow,\downarrow}. \quad (4)$$

The BICs are difficult to find because they are not coupled to the continuum energy spectra until the symmetry that allows them to exist is broken. For this reason, we calculate the conductance by varying the magnetic field and the Fermi energy. When the magnetic field is switched on, the BICs can be uncovered as an emerging resonance or antiresonance in the conductance. Once the presumed BICs are found, their spatially localized nature is assessed through the participation ratio (PR)

$$PR = \left(\sum_{n,m} |F_{nm}(E_{\text{BIC}})|^4 \right)^{-1}, \quad (5)$$

where F_{nm} is the amplitude of the normalized envelope function at site $\{n, m\}$. Notice that $PR = 1$ when the state is fully localized at a single site whereas $PR \simeq N$ for an extended state.

3. Results

We calculate the conductance numerically with the Kwant toolkit [39]. The parameters considered for the system and leads are the same as in the previous section. Additionally, the length for the horizontal and vertical dead-ends are $l_x = 8$ nm and $l_y = 10$ nm, respectively. The InSb nanowires chosen for this study have an electron effective mass $m_{\text{InSb}}^* = 0.014 m_e$ [40] and gyromagnetic factor $g_{\text{InSb}} \approx 50$ [41], where m_e is the free electron mass. The leads are also assumed to be InSb. For the simulations, the dimensions of the hashtag patterns was $L = 50$ nm for the length of the edges of the square. Finally, the grid spacing has been set to $a = 2$ nm.

3.1. Impact of the lead geometry

We will consider three configurationally different ways to attach the leads. The first one connects the leads into two opposite corners along the x direction. In the second one, the leads are connected one in front of the other along the x direction. In the third one, the leads are connected at two opposite corners but in perpendicular directions (see Fig. 1). The last geometry differs from the first one due to the effect of the magnetic field, which adds a phase difference between the two electron paths.

From Fig. 3(d), (e), and (f), we can see that all the configurations show a clear difference in the density of states when the magnetic field is applied for both spin projections since marked peaks appear at energies E_{BIC} . This change is due to the interaction that exists between the BICs and the continuum energy spectrum after applying the magnetic field. As anticipated, the presence of the BICs can be noticed in Figs. 3(a), (b) and (c), where the BIC at $E_{\text{BIC}} \approx 0.58$ eV is the more remarkable one as it is shared among all the configurations, as resonances or antiresonances in the conductance plots. For instance, the DOS around each BIC can be expressed as the superposition of two Lorentzian line shapes centered at energies ϵ_{\pm}

$$\rho(E) \approx \frac{1}{\pi} \left(\frac{\Gamma_+}{(E - \epsilon_+)^2 + \Gamma_+^2} + \frac{\Gamma_-}{(E - \epsilon_-)^2 + \Gamma_-^2} \right), \quad (6)$$

where Γ_+ and Γ_- stand for the width of the states strongly and weakly coupled to the continuum, respectively. As $\Gamma_- \rightarrow 0$ the DOS can written as

$$\rho(E) \approx \frac{1}{\pi} \frac{\Gamma_+}{(E - \epsilon_+)^2 + \Gamma_+^2} + \delta(E - \epsilon_-). \quad (7)$$

The Lorentzian line shapes centered at energy ϵ_- becomes a Dirac- δ function, a signature of the BIC. On the other hand, the conductance can be expressed as a convolution of Breit-Wigner and Fano line shapes in the following form

$$G(E) \approx \frac{\Gamma_+^2}{(E - \epsilon_+ - \Gamma_+)^2} \frac{|(E - \epsilon_-)/\Gamma_- + q|^2}{(E - \epsilon_-)^2/\Gamma_-^2 + 1}$$

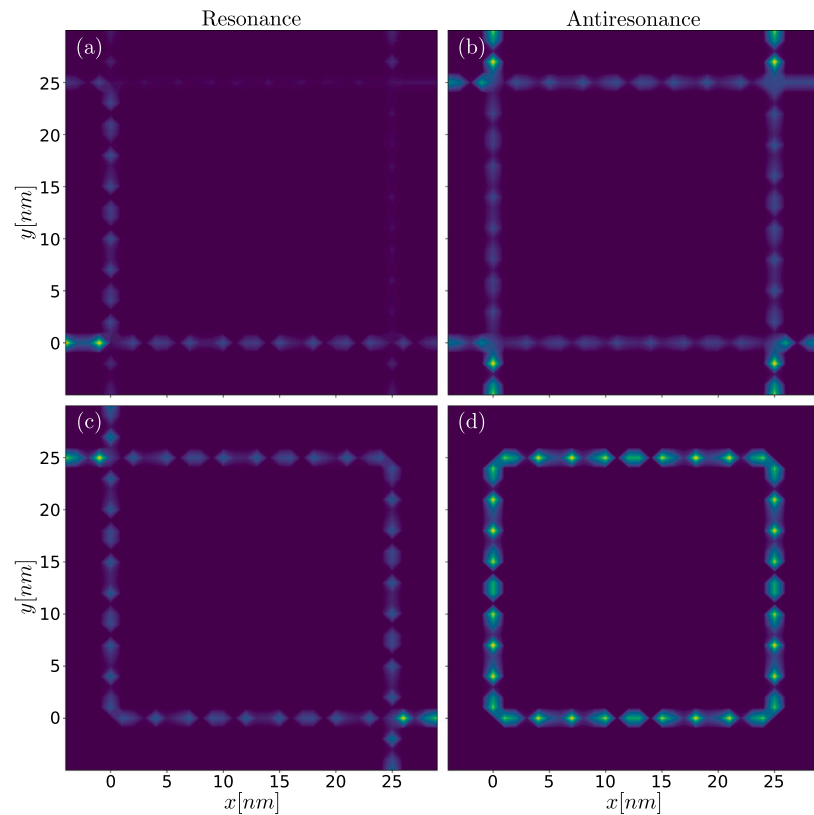


Fig. 4. Probability density for the structure shown in Fig. 1(a). The first (second) row displays the probability density in the absence (presence) of an external magnetic field. The first column shows the probability density at the energy where the resonance in the conductance occurs, $E \approx 0.54$ eV, while the second column is at $E \approx 0.58$ eV when there is an anti-resonance in the conductance. The higher the intensity of the color, the higher the probability density.

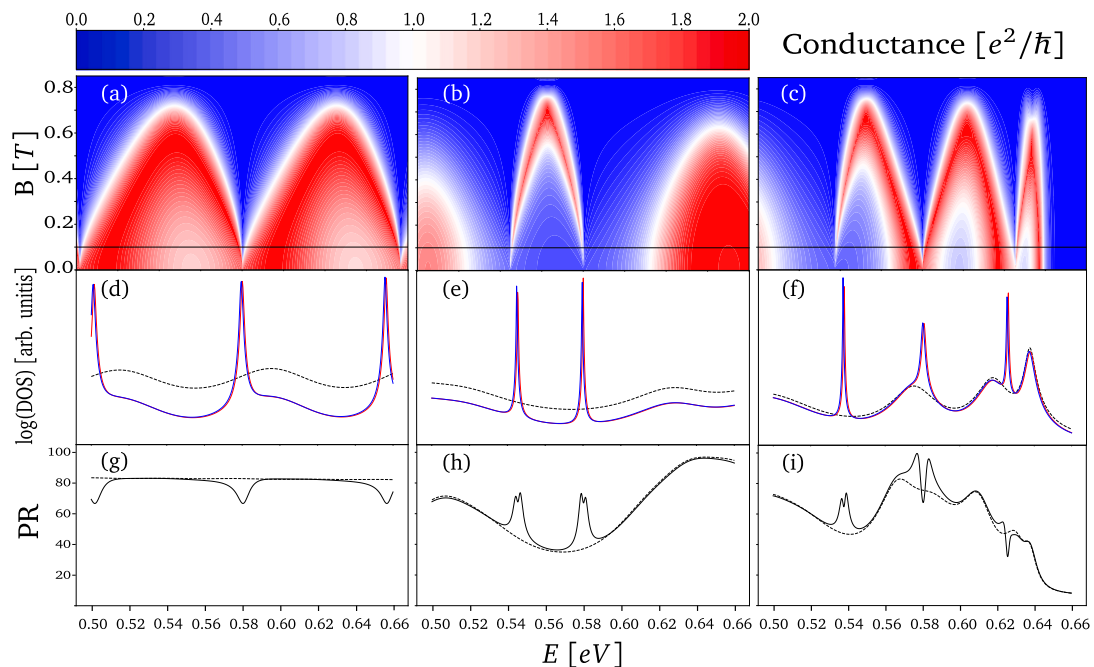


Fig. 5. Conductance of the nanowire network against the magnetic field B and the Fermi energy E . Panels (a), (b) and (c) correspond to the structures presented in Fig. 2(a), (b) and (c), respectively. The horizontal black line indicated the magnetic field at which the density of states and participation ratio are calculated ($B = 0.1$ T). Panels (d), (e) and (f) display the density of states with (solid line) and without (dashed line) magnetic field. Red (blue) line corresponds to the density of states with spin up (down). Panels (g), (h) and (i) represent the participation ratio with (solid line) and without (dashed line) magnetic field for the up spin projection. Panels (c), (f) and (i) present the same data as in Fig. 3(a), (e) and (h) to facilitate the comparison between the structures.

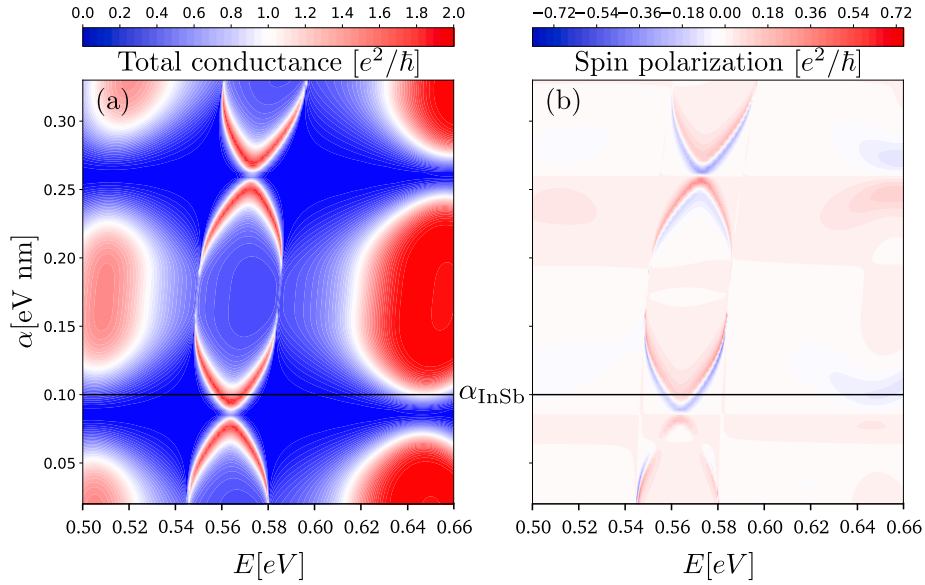


Fig. 6. (a) Conductance and (b) spin-dependent conductance of the nanowire network shown in Fig. 2(b) against the Rashba SOI α and the Fermi energy E when a perpendicular magnetic field is applied ($B = 0.1$ T). Here, positive values on the spin conductances mean that the up spin projection dominates the conductance. The black horizontal line represents the Rashba SOI estimated for InSb nanowires.

$$+ \frac{\eta^2}{(E - \epsilon_-)^2 + (\text{Im}(q)\Gamma_-)^2}, \quad (8)$$

where the Fano parameter q is a complex number and the parameter η is proportional to Γ_- .

To confirm that these peaks correspond to BICs, we have plotted the PR against the Fermi energy with and without magnetic field [Fig. 3(g), (h), and (i)]. Here, we can see that at the energy of the BICs, E_{BIC} , the PR is increased (decreased) when a resonance (anti-resonance) occurs in the conductance. This behavior is related with a delocalization (localization) of the state, as we can see qualitatively in Fig. 4. In addition, this behavior is followed by a higher increase of the PR in the vicinity of E_{BIC} , provoked by mixing the extended states with the BICs.

Although there are BICs in all the presented structure configurations, the first one will be the chosen lead's connection for the next section. This is because it have resonant-like BICs, that will be better resolved by experiments.

3.2. Impact of the system geometry

We will consider three different system geometries. The first geometry will have no dead-end chains resembling a square. In the second configuration, the scattering region will have only horizontal dead-end chains in each square corner. Finally, the last one will have either horizontal and vertical dead-end chains in each corner of the square (see Fig. 2). From the density of states shown in Fig. 5, we realize that BICs emerge in all the considered geometries, either as resonances or anti-resonances. BICs are better revealed in an energy window where the conductance is zero in the absence of an applied magnetic field, and some resonances appear after its application; these resonances will correspond to the BICs. Therefore, the most favorable configuration to detect the occurrence of BICs is the structure shown in Fig. 2(b). Moreover, it is noticeable that the BIC at $E_{\text{BIC}} \approx 0.58$ eV is again shared in all the structures. For this reason, this will be the geometry and energy studied in the following section.

3.3. Impact of the Rashba SOI

In previous calculations, we have neglected the Rashba SOI ($\alpha = 0$). In Fig. 6, we show the evolution of the BICs against the magnitude of

the Rashba SOI and the Fermi energy when a magnetic field is applied. This figure shows that the Rashba SOI smears out the resonances, making the BICs harder to identify. In addition, we can see an oscillatory behavior on increasing α , associated with the Aharonov–Casher effect [42]. InSb nanowires have a Rashba SOI of the order of $\alpha_{\text{InSb}} = 0.1$ eV [43], which is not the optimum value for observing the BICs. For this reason, an external electric field might be necessary to change α , therefore facilitating the observation of the BICs. Additionally, we can see that the nanowire network can be used in spintronics because it displays a non-zero spin conductance at some specific energies. Also, with the applied electric field, we can control which spin projection will be dominant, allowing us to use them as spin filters.

3.4. Quality factor

Finally, to evaluate the effectiveness of the BICs to tailor the transport properties of the nanowire network, we will calculate the quality factor (Q-factor) $Q = \epsilon_-/\Gamma_-$ for one of the BICs analyzed in the previous section. Specifically, we will examine the evolution of the resonance width Γ_- at $E = 0.58$ eV in the DOS when the magnetic field increases, fitting the results to the second term of Eq. (6). From Fig. 7 we can see that the resonance becomes broader and shifts towards lower energies as the magnetic field is increased. The inset of Fig. 7 demonstrated that the Q-factor scales as $Q \sim 1/B^\nu$ with $\nu \simeq 1.2$ as a function of the magnetic field. Although our simulations predict that the Q-factor increases without bound on decreasing the magnetic field, in an experiment the broadening of the resonance should be of the order of the thermal broadening or inhomogeneous broadening (e.g. due disorder scattering) for the BICs to have an impact on the conductance, imposing a lower limit to the magnetic field.

4. Conclusions

In this article, we have proposed a setup that could be used to search for BICs in electronic experiments. We have shown that the hashtag nanowire networks will reveal the BICs as resonances or antiresonances of the conductance by varying the magnetic field and the Fermi energy. This statement is supported by calculating the density of states whose peaks associated with BICs broaden upon rising the magnetic field, i.e., increasing the coupling to the extended states of the continuum

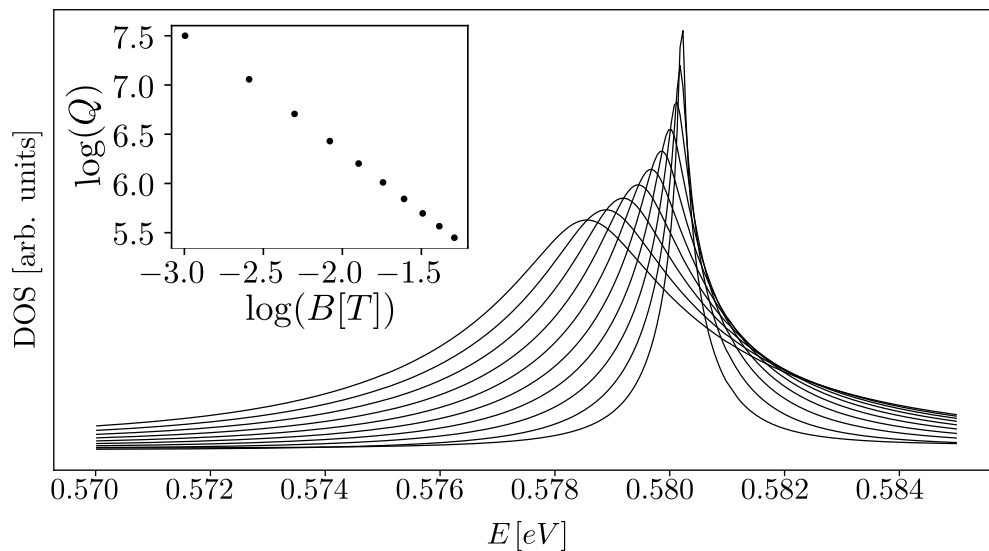


Fig. 7. Density of states of the BIC located at $E = 0.58$ eV of the nanowire network shown in Fig. 2 (b) for different values of magnetic field against the Fermi energy E . In the inset the Q-factor is displayed against the magnetic field.

energy spectrum. In addition, we have studied different configurations to elucidate the best one for uncovering BICs. The study showed that the optimum geometry is the one with horizontal dead-end chains connected to each corner and the leads connected horizontally to opposite corners. Hereafter, we studied the impact of the Rashba SOI on the BICs. We found that this interaction blurs the BICs, making them harder to find. However, it opens a way to use hashtag-like nanowire networks in spintronics as spin filters while tuning the Rashba SOI by strain or applied electric field. Finally, we studied the Q-factor of one of the BICs to assess the impact on the conductance in real devices.

CRedit authorship contribution statement

D. Martínez: Writing – original draft, Visualization, Methodology, Investigation, Formal analysis, Data curation, Conceptualization. **P.A. Orellana:** Writing – original draft, Conceptualization. **L. Rosales:** Writing – original draft. **J. Dolado:** Supervision, Conceptualization. **M. Amado:** Writing – original draft, Supervision, Conceptualization. **E. Díez:** Writing – original draft, Supervision, Conceptualization. **F. Domínguez-Adame:** Writing – original draft, Supervision, Funding acquisition, Formal analysis, Conceptualization. **R.P.A. Lima:** Writing – original draft, Visualization, Supervision, Methodology, Investigation, Formal analysis, Conceptualization.

Declaration of competing interest

The authors declare that they have no known competing financial interests or personal relationships that could have appeared to influence the work reported in this paper.

Acknowledgments

We acknowledge financial support from Comunidad de Madrid (Recovery, Transformation and Resilience Plan) and NextGenerationEU from the European Union (Grant MAD2D-CM-UCM5), Agencia Estatal de Investigación of Spain (Grant PID2022-136285NB-C31/2), Junta de Castilla y León and The European Regional Development Fund (SA106P23) and FONDECYT (Grants 1220700 and 1201876). J. D. acknowledges the financial support of ESRF for his postdoctoral fellowship position

Appendix A. Supplementary data

Supplementary material related to this article can be found online at <https://doi.org/10.1016/j.physe.2024.116145>.

Data availability

Data will be made available on request.

References

- [1] J. von Neumann, E. Wigner, On some peculiar discrete eigenvalues, *Phys. Z.* 30 (1929) 465.
- [2] F.H. Stillinger, D.R. Herrick, Bound states in the continuum, *Phys. Rev. A* 11 (1975) 446.
- [3] H. Friedrich, D. Wintgen, Physical realization of bound states in the continuum, *Phys. Rev. A* 31 (1985) 3964–3966.
- [4] J.M. Zhang, D. Braak, M. Kollar, Bound states in the continuum realized in the one-dimensional two-particle hubbard model with an impurity, *Phys. Rev. Lett.* 109 (2012) 116405.
- [5] Y. Plotnik, O. Peleg, F. Dreisow, M. Heinrich, S. Nolte, A. Szameit, M. Segev, Experimental observation of optical bound states in the continuum, *Phys. Rev. Lett.* 107 (2011) 183901.
- [6] A. Cerjan, C. Jörg, S. Vaidya, S. Augustine, W.A. Benalcazar, C.W. Hsu, G. von Freymann, M.C. Rechtsman, Observation of bound states in the continuum embedded in symmetry bandgaps, *Sci. Adv.* 7 (2021) eabk1117.
- [7] Y. Wang, B.-Y. Xie, Y.-H. Lu, Y.-J. Chang, H.-F. Wang, J. Gao, Z.-Q. Jiao, Z. Feng, X.-Y. Xu, F. Mei, S. Jia, M.-H. Lu, X.-M. Jin, Quantum superposition demonstrated higher-order topological bound states in the continuum, *Light Sci. Appl.* 10 (2021) 173.
- [8] S. Joseph, S. Pandey, S. Sarkar, J. Joseph, Bound states in the continuum in resonant nanostructures: An overview of engineered materials for tailored applications, *Nanophotonics* 10 (2021) 4175.
- [9] T. Shi, Z.-L. Deng, G. Geng, X. Zeng, Y. Zeng, G. Hu, A. Overvig, J. Li, C.-W. Qiu, A. Alù, Y.S. Kivshar, X. Li, Planar chiral metasurfaces with maximal and tunable chiroptical response driven by bound states in the continuum, *Nature Commun.* 13 (2022) 4111.
- [10] L. Liu, T. Li, Q. Zhang, M. Xiao, C. Qiu, Universal mirror-stacking approach for constructing topological bound states in the continuum, *Phys. Rev. Lett.* 130 (2023) 106301.
- [11] S.I. Azzam, V.M. Shalaev, A. Boltasseva, A.V. Kildishev, Formation of bound states in the continuum in hybrid plasmonic-photonic systems, *Phys. Rev. Lett.* 121 (2018) 253901.
- [12] Y. Liang, K. Koshelev, F. Zhang, H. Lin, S. Lin, J. Wu, B. Jia, Y. Kivshar, Bound states in the continuum in anisotropic plasmonic metasurfaces, *Nano Lett.* 20 (2020) 6351.
- [13] S. Sun, Y. Ding, H. Li, P. Hu, C.-W. Cheng, Y. Sang, F. Cao, Y. Hu, A. Alù, D. Liu, Z. Wang, S. Gwo, D. Han, J. Shi, Tunable plasmonic bound states in the continuum in the visible range, *Phys. Rev. B* 103 (2021) 045416.

- [14] Q. Song, Z. Yi, Z. Zhou, Evolution of merging bound states in the continuum at Γ point in parameter space, *Phys. Rev. A* 109 (2024) 023525.
- [15] I. Deriy, I. Toftul, M. Petrov, A. Bogdanov, Bound states in the continuum in compact acoustic resonators, *Phys. Rev. Lett.* 128 (2022) 084301.
- [16] Z. Pu, H. He, L. Luo, Q. Ma, L. Ye, M. Ke, Z. Liu, Acoustic higher-order Weyl semimetal with bound hinge states in the continuum, *Phys. Rev. Lett.* 130 (2023) 116103.
- [17] J. Jincheng, L. Jiuyang, W. Deng, X. Huang, Z. Liu, Acoustic bound states in continuum protected by crystalline symmetry, *Europhys. Lett.* 143 (2023) 26002.
- [18] D. Lee, J. Park, S. Kim, J. Mun, J. Kim, X. Piao, N. Park, J. Rho, Elastic bound states in the continuum by acoustoelastic interaction, *Extreme Mech. Lett.* 61 (2023) 101965.
- [19] M.L. Ladrón de Guevara, P.A. Orellana, Electronic transport through a parallel-coupled triple quantum dot molecule: Fano resonances and bound states in the continuum, *Phys. Rev. B* 73 (2006) 205303.
- [20] E.N. Bulgakov, K.N. Pichugin, A.F. Sadreev, I. Rotter, Bound states in the continuum in open Aharonov-Bohm rings, *JETP Lett.* 84 (2006) 430–435.
- [21] C. González-Santander, P.A. Orellana, F. Domínguez-Adame, Bound states in the continuum driven by AC fields, *Europhys. Lett.* 102 (2013) 17012.
- [22] N. Prodanović, V. Milanović, Z. Ikonić, D. Indjin, P. Harrison, Bound states in continuum: Quantum dots in a quantum well, *Phys. Lett. A* 377 (2013) 2177.
- [23] J. Mur-Petit, R.A. Molina, Chiral bound states in the continuum, *Phys. Rev. B* 90 (2014) 035434.
- [24] B. Grez, J.P. Ramos-Andrade, V. Juričić, P.A. Orellana, Bound states in the continuum in a two-channel Fano-Anderson model, *Phys. Rev. A* 106 (2022) 013719.
- [25] C.W. Hsu, B. Zhen, A.D. Stone, J.D. Joannopoulos, M. Soljačić, Bound states in the continuum, *Nat. Rev. Mater.* 1 (2016) 16048.
- [26] K.L. Koshelev, Z.F. Sadrieva, A.A. Shcherbakov, Y.S. Kivshar, A.A. Bogdanov, Bound states in the continuum in photonic structures, *Phys.-Usp.* 66 (2023) 494.
- [27] M. Kang, T. Liu, C.T. Chan, M. Xiao, Applications of bound states in the continuum in photonics, *Nat. Rev. Phys.* 5 (2023) 659.
- [28] G. Xu, H. Xing, Z. Xue, D. Lu, J. Fan, J. Fan, P.P. Shum, C. Longqing, Recent advances and perspective of photonic bound states in the continuum, *Ultrafast Sci.* 3 (2023) 0033.
- [29] D.C. Marinica, A.G. Borisov, S.V. Shabanov, Bound states in the continuum in photonics, *Phys. Rev. Lett.* 100 (2008) 183902.
- [30] E.N. Bulgakov, A.F. Sadreev, Bound states in the continuum in photonic waveguides inspired by defects, *Phys. Rev. B* 78 (2008) 075105.
- [31] E.N. Bulgakov, A.F. Sadreev, Bound states in photonic Fabry-Perot resonator with nonlinear off-channel defects, *Phys. Rev. B* 81 (2010) 115128.
- [32] A. Albo, D. Fekete, G. Bahir, Electronic bound states in the continuum above (Ga,In)(As,N)/(Al,Ga)As quantum wells, *Phys. Rev. B* 85 (2012) 115307.
- [33] J.U. Nöckel, Resonances in quantum-dot transport, *Phys. Rev. B* 46 (1992) 15348.
- [34] U. Fano, Effects of configuration interaction on intensities and phase shifts, *Phys. Rev.* 124 (1961) 1866.
- [35] R.L.M. Op het Veld, D. Xu, V. Schaller, M.A. Verheijen, S.M.E. Peters, J. Jung, C. Tong, Q. Wang, M.W.A. de Moor, B. Hesselmann, K. Vermeulen, J.D.S. Bommer, J. Sue Lee, A. Sarikov, M. Pendharkar, A. Marzegalli, S. Koelling, L.P. Kouwenhoven, L. Miglio, C.J. Palmstrøm, H. Zhang, E.P.A.M. Bakkers, In-plane selective area InSb-Al nanowire quantum networks, *Commun. Phys.* 3 (2020) 59.
- [36] Y. Oreg, G. Refael, F. von Oppen, Helical liquids and Majorana bound states in quantum wires, *Phys. Rev. Lett.* 105 (2010) 177002.
- [37] A. Stern, N.H. Lindner, Topological quantum computation—from basic concepts to first experiments, *Science* 339 (2013) 1179.
- [38] M.L.L.d. Guevara, F. Claro, P.A. Orellana, Ghost Fano resonance in a double quantum dot molecule attached to leads, *Phys. Rev. B* 67 (2003) 195335.
- [39] C.W. Groth, M. Wimmer, A.R. Akhmerov, X. Waintal, Kwant: a software package for quantum transport, *New J. Phys.* 16 (2014) 063065.
- [40] W. Zawadzki, Electron transport phenomena in small-gap semiconductors, *Adv. Phys.* 23 (1974) 435.
- [41] H.A. Nilsson, P. Caroff, C. Thelander, M. Larsson, J.B. Wagner, L.-E. Wernersson, L. Samuelson, H.Q. Xu, Giant, level-dependent g factors in InSb nanowire quantum dots, *Nano Lett.* 9 (2009) 3151.
- [42] M. König, A. Tschetschetkin, E.M. Hankiewicz, J. Sinova, V. Hock, V. Daumer, M. Schäfer, C.R. Becker, H. Buhmann, L.W. Molenkamp, Direct observation of the Aharonov-Casher phase, *Phys. Rev. Lett.* 96 (2006) 076804.
- [43] I. van Weperen, B. Tarasinski, D. Eeltink, V.S. Pribiag, S.R. Plissard, E.P.A.M. Bakkers, L.P. Kouwenhoven, M. Wimmer, Spin-orbit interaction in InSb nanowires, *Phys. Rev. B* 91 (2015) 201413.